JOURNAL OF MATERIALS SCIENCE 22 (1987) 722–736

Chemisorption mechanism and effect of polyacrylic acid on the improvement in bond durability of zinc phosphate-to-polymer adhesive joints

T. SUGAMA, L. E. KUKACKA, N. CARCIELLO, J. B. WARREN
Process Sciences Division, Department of Applied Science, Brookhaven National Laboratory, Associated Universities, Inc., Upton, Long Island, New York 11973, USA

It has been found that the outermost surface sites of polyacrylic acid-complexed crystalline zinc phosphate layers precipitated on cold-rolled steel surfaces act significantly to promote interfacial adhesive bonding to polymeric topcoats. This is the result of electrostatic internal diffusion and segmental chemisorption mechanisms of polyelectrolyte macromolecules either on newly precipitated crystal nuclei or on crystal growth sites during the primary zinc phosphate conversion process. The nature of the polymer-to-polymer chemical bond produced at the polymer-to-complex zinc phosphate precoat interfacial joints plays the key role in the achievement of long-term bond durability upon exposure to chemically corrosive environments. The locus of adhesive loss at the polymer-to-complex zinc phosphate joints after exposure to a hot acid solution was clearly identified to be cohesive failure in the crystalline precoat layers. A stable bond resulted from the formation of an interfacially produced hydrophobic structure by interactions between the polymer and the functional organic species existing on the complex precoat surfaces. The chemisorbed polyelectrolytes also served chemically to couple the organic coating and the inorganic zinc phosphate conversion layer.

1. Introduction

In earlier work of this laboratory [1, 2] it has been demonstrated that when mild carbon cold-rolled steels are immersed in zinc orthophosphate dihydrate-based phosphating solutions, the resultant crystalline zinc phosphate conversion layer deposited on the steel substrate surface consists of a highly dense configuration of large rectangular-type crystals $\sim 420\,\mu m$ in length and $\sim 120\,\mu m$ thick. The surface topographical features of the zinc phosphate conversion precoat were characterized by a dendritic microstructure array comprised of interlocking rectangular crystals of insoluble zinc phosphate hydrate. The open surface structure of the interlocked crystal layers contributed significantly to the formation of a strong mechanical interlocking reaction with the polymeric topcoat systems, thereby enhancing the magnitude of the adhesive force at the precoat–topcoat interfaces. Although this well-crystallized zinc phosphate precoat appeared to be suitable as a corrosion barrier for the substrate, the fragile characteristics of this bulky crystal structure lead to failure during flexure or other deformation of the substrate. Deformation failures of layers having low stiffness characteristics appear to be directly related to the development of micropores and fissures which reduce the effectiveness of the corrosion-resistant coatings. These characteristics lead to a high oxygen and moisture availability at the substrate surface and progressively promote a cathodic delamination reaction. The hydroxyl ions generated by the cathodic reactions induce an alkaline condition which causes delamination at the precoat–substrate interface [3–5]. Thus, an increase in the flexural modulus of the crystalline conversion layer itself is of considerable importance when the physical deformation characteristics of the metal substrate are considered.

In an attempt to suppress the physical deformation failures of the well-crystallized precoats, various polyelectrolyte macromolecules were introduced into the basic zinc phosphating formula. These were found to produce crystal conformations and configurations which improve the stiffness and toughness properties of the conversion layers. The polyelectrolytes used include such diverse polymers as proteins, nucleic acid, polyacrylic acid, polyphosphates, and polyvinylpyridinium chloride. The addition of an appropriate amount of polyacrylic acid (PAA) macromolecules from among these polyelectrolytes was especially effective in improving the controllability of the crystal dimensions, the extent of crystallinity, and the coating weight of the zinc phosphate layers [6].

The incorporation of polyelectrolytes as a means of inhibiting the rate of nucleation and crystal growth from supersaturated solutions of inorganic compounds is not a new idea. As noted by Crawford [7]

0022–2461/87 $03.00 + .12

and Nestler [8], PAA and polyphosphate inhibitors have been shown to be active in reducing the crystallization rate of calcium sulphate dihydrate. This was interpreted in terms of adsorption of the polyelectrolyte on the crystal embryos (nuclei smaller than the critical size) of $CaSO_4 \cdot 2H_2O$ occurring during the crystallization process. The marked changes in crystal morphology and habit by PAA contributed to the findings of the physicochemical factors governing the increase in mechanical properties of PAA-modified zinc phosphate complex layers. Consequently, the mechanical behaviour of the complex layers depended primarily upon the thickness, fineness, and density of the coatings, and the average molecular weight (MW) of the macromolecules. The use of PAA macromolecules with a high MW of 1×10^5 resulted in the most effective complex crystal formation and dimensions for achieving the ultimate flexural modulus [9].

The stiff complex crystal precoat layer and surface not only provide a corrosion barrier on the substrates, but also possess the ability to promote adhesive bonds at polymeric topcoat–complex precoat joints. The latter is due to the presence of a thin functional PAA polymer film at the outermost surface sites of the precoat layers. This improved interfacial adhesion leads to an enhancement of the durability of the joints.

In order to estimate the approximate durability for certain applications, polymer-coated substrates are often exposed to hot water at 80 to 100° C. When the adhesion is poor, the coating–substrate bond deteriorates immediately upon exposure. The loss in adhesion, which most commonly occurs as the result of the formation of blisters, can be explained as the result of an osmotic mechanism. As water penetrates through the coating to the interface, a concentrated solution is developed with sufficient osmotic force to drive water from the coating surface to the interface, and a blister is formed [10]. The blister provides a locale for the collection of water at the interface. Oxygen also penetrates through the coating, and ionic materials are leached from the interface. All these constituents are then available for the electrochemical cathodic delamination reaction described previously. Certain exceptional cases have been pointed out in the literature in which cathodic disbonding was related to acid or complexing media in which ferrous ion is soluble [11].

Accordingly, an aim of the present study was to investigate the surface and subsurface characteristics of the complex precoat which is responsible for enhancing the durability of polymer-to-complex crystal adhesion when subjected to a hot acidic solution at 80° C, and to postulate a comprehensive failure mode and disbondment locus. The former has been explored using a combination of highly sensitive surface, subsurface, and solid analytical techniques such as electron spectroscopy for chemical analysis, Auger electron spectroscopy, and X-ray powder diffraction. The quantitative analysis of chemical elements by energy-dispersive X-ray spectrometry coupled with low-resolution scanning electron microscopy offers a high potential for acquiring information regarding failure modes.

2. Experimental procedures

2.1. Materials

The metal substrate used in the experiments was mild carbon cold-rolled steel containing 0.23 wt % C, 0.6 wt % Mn, 0.15 wt % Si, and $\leqslant 0.04$ wt % P. The zinc phosphate-convertible liquid was composed of 5 parts zinc orthophosphate dihydrate and 95 parts 10% H_3PO_4 in conjunction with a 9.5% PAA solution by weight of the total phosphating mass. Commercial PAA, 25% solution in water, having an average molecular weight (MW) of 104 000 was supplied by Scientific Polymer Products, Inc. An array of the PAA–zinc phosphate composite conversion layers having crystal dimensions of micron orders on the substrate surfaces was prepared in accordance with the following immersion sequence. The clean metal substrates were first rinsed with an organic solvent, and then immersed for ~ 7 h in the coating solution described above at a temperature of 80° C. After depositing the composite conversion layers, the substrates were placed in an oven at 150° C for ~ 5 h to remove all moisture from the precoat surfaces and to solidify the PAA macromolecule complexed with zinc phosphate crystals. After baking, the surface topography of the PAA–zinc phosphate composite conversion layers deposited on the steel surface typically resembles the microscopic representation in Fig. 1.

Commercial-grade polyurethane (PU) M313 resin, supplied by the Lord Corporation, was applied as an elastomeric topcoating. Silica flour filler (size < 0.074 mm), which is generally used as a pigment in organic coatings, was employed as a reinforcement in the films. The concentration of the pigment added to the PU resin was 20 wt %. The polymerization of silica-filled PU composite was initiated by incorporating a 50% aromatic amine curing agent M201. The initiated topcoat system was then cured in the oven at a temperature of 80° C.

2.2. Measurements

Electron spectroscopy for chemical analysis (ESCA) was employed for identifying the chemical states and elemental compositions at the surface sites of PAA–zinc phosphate composite layers. These studies were completed using the Perkin-Elmer PHI Model 550 ESCA/SAM, (scanning Auger microprobe) equipped with a magnesium X-ray source.

Auger electron spectroscopy combined with ion sputter-etching was used in depth-composition profiling studies to detect interdiffusion of elemental composition at internal interfaces in the PAA-adsorbed zinc phosphate layers. This study was conducted using a Perkin-Elmer PHI Model 610 Scanning Auger Microprobe.

The zinc phosphate conversion products deposited on the treated metal surface were identified by X-ray powder diffraction analyses. To prepare the fine powder samples, the deposited conversion layers were removed by scraping the surfaces and were then ground to a size of ~ 325 mesh (0.044 mm).

Peel strength tests of adhesive bonds at the polyurethane topcoat-modified metal substrate interfaces were conducted at a separation angle of $\sim 180°$ and a

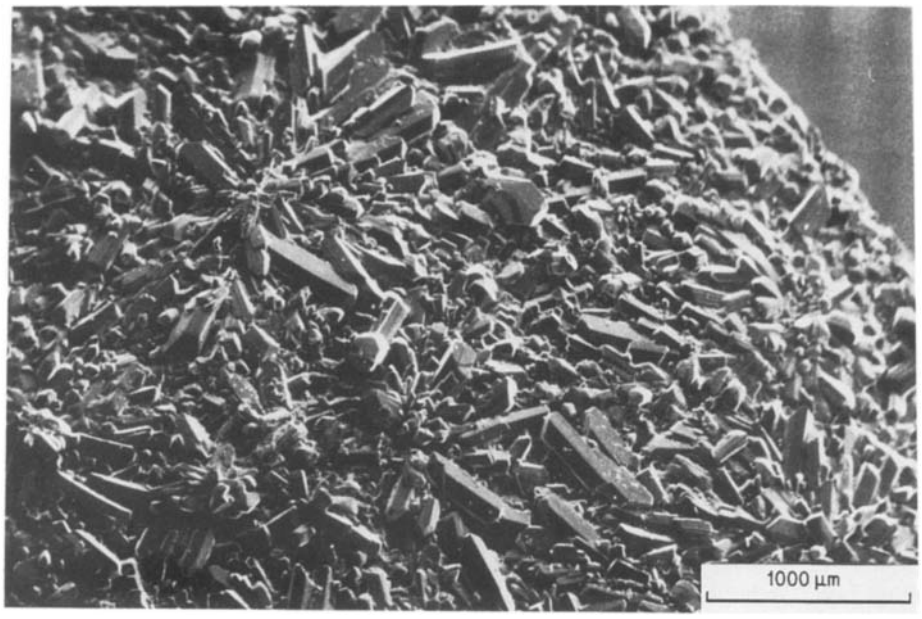

Figure 1 Topographical features of PAA–zinc phosphate complex crystals deposited on a carbon steel surface.

crosshead speed of 5 cm min^{-1}. The test specimens consisted of one piece of flexible polyurethane topcoat, 2.5 by 30.5 cm, bonded for 15.2 cm at one end to one piece of flexible or rigid substrate material, 2.5 by 20.3 cm, with the unbonded portions of each member being face to face. The thickness of the polyurethane topcoat overlaid on the complex crystal surfaces was ~0.95 mm.

An AMR 10 nm scanning electron microscopy associated with TN-2000 energy-dispersive X-ray spectrometry was used to inspect the adhesion failure mode and locus at the interfaces.

3. Results and discussion

3.1. Surface and subsurface

Electron spectroscopy for chemical analysis (ESCA) was used to examine the PAA–zinc phosphate complex surfaces. Auger electron spectroscopy (AES) was employed for the depth-composition profile studies of the complex layers at depths up to 300 nm.

The ESCA survey scan, to identify elements at the outermost surface sites, is shown in Fig. 2. Carbon oxygen atoms appear as major lines, and zinc and phosphorus as minor ones. The chemical states of zinc and phosphorus are assigned to the presence of the zinc and phosphorus compounds, and the carbon may be attributed to the organic PAA macromolecules and carbonate. The oxygen atom is related to both the zinc phosphate compounds and the polyelectrolyte.

To substantiate the chemical state information for these elements, high-resolution ESCA spectra was obtained from the complex surfaces. Fig. 3 shows typical survey spectra of the zinc $2p^{1/2}$ and $2p^{3/2}$ core levels. The spectra which are characterized by binding energies at 1046.5 eV for the $2p^{1/2}$ line and at 1022.7 eV for the $2p^{3/2}$, reveal the presence of oxidized zinc and metallic zinc. It is generally known that the chemical shift for the Zn $2p^{3/2}$ photoelectron line from metallic to oxidized zinc is less than 1 eV. Thus, the Auger parameter was used to identify the source of the zinc formations. The Auger parameter (α) has been defined by the following equation [12]:

$$\alpha = KE_a - KE_p = BE_p - BE_a \qquad (1)$$

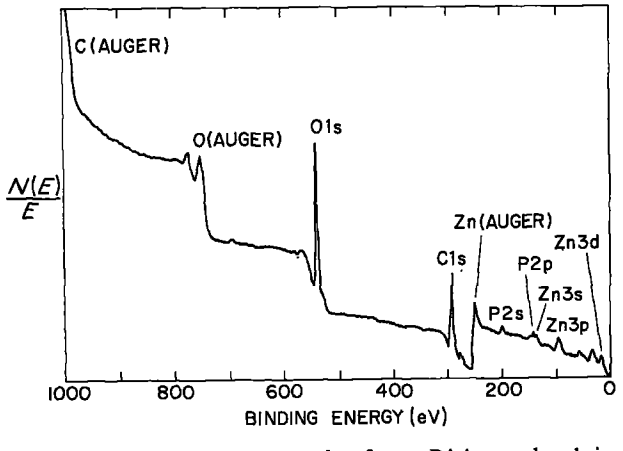

Figure 2 ESCA survey spectrum taken from a PAA-complexed zinc phosphate conversion precoating surface.

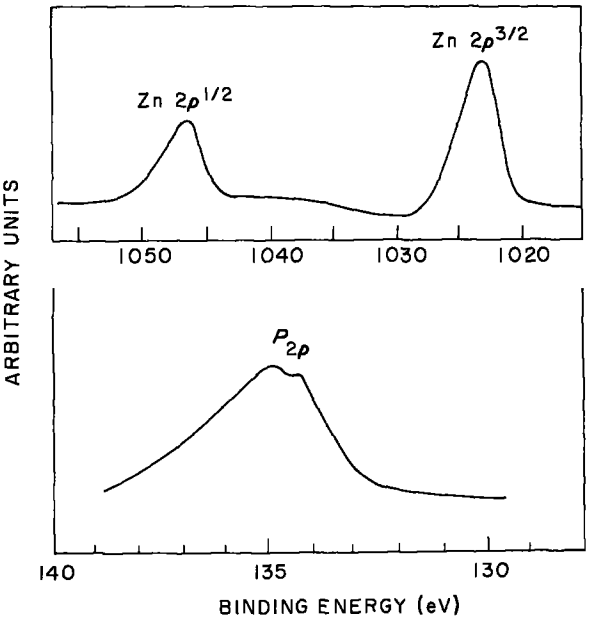

Figure 3 Spectra of Zn $2p^{1/2}$ and Zn $2p^{3/2}$, and P $2p$ of complex precoat surface.

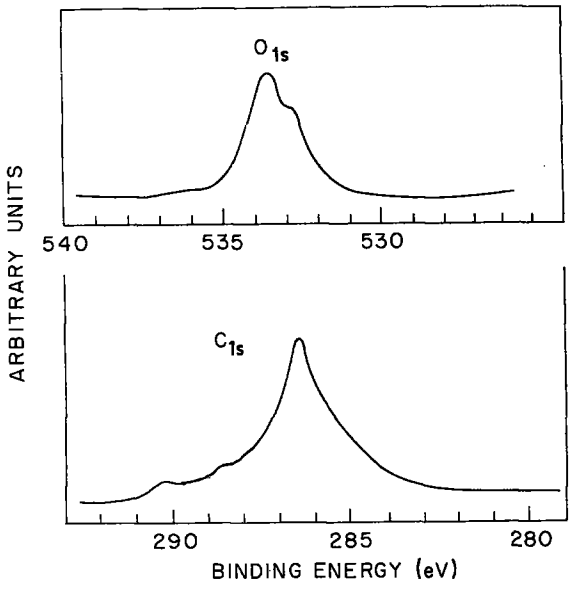

Figure 4 Oxygen and carbon 1s spectra from PAA-modified zinc phosphate surface.

where KE_a is the kinetic energy of the auger line, KE_p is the photoelectron kinetic energy, and BE_p and BE_a refer to the binding energies of photoelectron and auger lines, respectively. In dealing with the Fermi level, BE_a is given by

$$BE_a = h\nu - KE_p \quad (2)$$

where $h\nu$ is the photon energy. Equations 1 and 2 can be combined and written as follows

$$KE_a + BE_p = h\nu + \alpha \quad (3)$$

Values for the parameters KE_a and BE_p were obtained from the L M M and the $2p^{3/2}$ lines in the Zn spectrum: KE_a = 987.4 eV and BE_p = 1022.7 eV. Thus, the sum of the photon energy and the Auger parameter was equal to the value of 2010.1 eV. Using the Auger parameter plot from [13], the source of the zinc was definitely identified as the ZnO.

The phosphorus 2*p* line is also exhibited in Fig. 3. The spectra indicate photoelectron peaks at two levels of adsorption in the binding energy range of 136 to 134 eV. The value of 135.1 eV is likely to indicate the presence of phosphorus pentoxide, P_2O_5, while that on around 134.3 eV suggests the presence of metaphosphoric acid, HPO_3. The HPO_3 may be formed by dihydration of orthophosphoric acid existing on the complex layer surface during the baking processes at high temperature. The presence of both ZnO and P_2O_5 obviously represents the existence of zinc phosphate compounds at the outermost surface sites.

The ESCA signatures of oxygen and carbon 1 s core levels are given in Fig. 4. A high-resolution examination of the oxygen 1s region revealed the presence of two distinct types of oxygen-containing species. The conspicuous peak at 533.7 eV is attributed to the oxygen atoms in the carboxylate and cyclic linkage formed by the intra-dehydration reaction. The oxygen of the carbonyl bond has a lower binding energy than the single bonded oxygen which is a less effective negative character. Thus, the shoulder at 532.9 eV was assigned to the C=O group, possibly an inorganic oxygen species such as P–O or Zn–O bonds.

Inspection of the C_{1s} regions indicated the presence of at least three different carbon species in the spectrum. A sharp singlet at 286.5 eV and two weak peaks at ~288.6 and 290.3 eV are evident. The former is due to the CH_2 of alkane line contribution expressed in terms of the backbone carbon and the cyclic linkage carbon. The carbon associated with the carboxyl group is at the higher binding energy since the effective positive charge on this carbon is due to the strong electron withdrawing influence of the double bond to oxygen. Hence, the central carbon peak is probably related to the carbonyl-type carbon in the pendent carboxyl groups. The highest assignment near 290.3 eV is very likely associated with oxidized carbon species. These residue species may include ionic carboxylate, free carboxylic acid, and small amounts of carbonate. The presence of carbonates may result in the adsorption of atmospheric carbon dioxide by residual hydroxides in the crystal precoating. Therefore, the outermost surface appears to be composed of a hybrid formation of multiple constituents such as ZnO, P_2O_5, HPO_3, and functional organic species. When the polymeric topcoating systems are overlaid on the crystal precoat surface, it can be inferred that the presence of the functional organic species leads to the formation of strong chemical bonds with the polymer topcoats.

It is important to know not only what is present at the surface sites of the conversion layers, but also how the chemical composition varies as a function of depth. Information regarding the depth-composition profile was obtained using Auger electron spectroscopy (AES) in conjunction with ion sputter-etching. In this analysis, an ~60 μm thickness of a PAA–zinc phosphate composite layer was used (see Fig. 5). The resulting profile, shown in Fig. 6, was plotted as atomic concentration versus sputter time. The sputter rate for the depth profiling was ~1 nm min^{-1}. The profile which was obtained in ~300 min using simultaneous sputtering and analysis, permits a rapid indentification of layer constituents and structure. Not surprisingly, the predominant element detected at a sputter time of ~3 min is carbon which ascribes to the presence of the organic species and carbonaceous materials. The carbon signal intensity is significantly reduced as the sputtering time is increased until the concentration stabilizes at a value of ~9% after ~40 min. This value is less than 15% of the original concentration at the outermost surface sites. Of particular interest is the constant amount of carbon in the depth range of ~40 to ~300 nm. This indicates that the polyelectrolyte was chemisorbed regularly on the crystal faces throughout the conversion layers, thereby contributing to the transformation of the crystal precoat from a brittle to a plasticized nature.

The oxygen content increases monotonically with the sputtering time and levels off at a depth of ~50 nm. The maximum value of ~56% corresponds to more than twice that of the original content on the surface. The concentrations of other elements such as zinc and phosphorus, which are present in very small quantities at the surface sites, also increased with elapsed sputter times until reaching a constant value

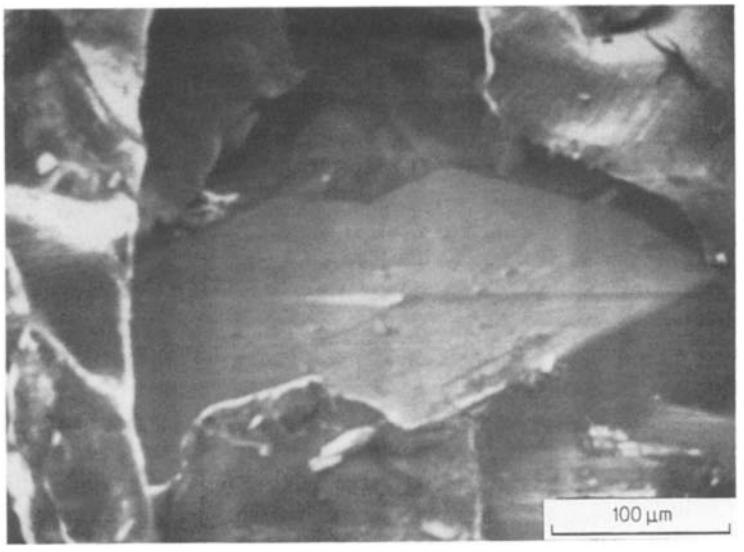

Figure 5 Target crystal for depth-composition profile of complex precoat layer using Auger survey spectra.

after ~50 min. This implies that the quality of zinc phosphate crystal formed within the first ~40 nm depth is inferior because of the chemisorption of highly concentrated PAA on the crystals.

In conjunction with the results of an ESCA surface survey, the presence of iron at the outermost surface of an ESCA surface sites could not be identified on the AES profile. However, as these surface elements are removed, the iron signal slowly grows with increased etching times and reaches a constant value of ~7.5% within ~40 min. Even though the concentration of iron below the surface is smaller than the concentrations for the other elements, the fact that the presence of iron coincides with the presence of phosphorus throughout the profile suggests that iron phosphate compounds exist as a minor phase in the zinc phosphate layers. The converted iron compounds probably involve iron phosphate, Fe $(H_2PO_4)_2$, and phosphophyllite [$Zn_2Fe\ (PO_4)_2 \cdot 4H_2O$)], in which some zinc is replaced by iron atoms. It is speculated that these iron-based phosphate compounds can be produced by an electrochemical reaction in the induction periods at the metal–solution interfaces.

From the above results, it can be concluded that the PAA macromolecules exist throughout the first ~5 nm of the layer. The poorly crystallized zinc and iron phosphate formations caused by chemisorbing the abundant polyelectrolyte are present at depths ranging from ~5 to 35 nm. Well-crystallized phosphate phases in the presence of a small amount of PAA were identified to be > 35 nm below the surface. However, the elemental analyses at depths > 300 nm were not performed. It is important that future work should include a quantitative elemental survey at the interface between the PAA-adsorbed crystal and the metal substrate so that additional information regarding the adhesion mechanisms at the crystal-to-substrate interfacial joints can be obtained.

On the basis of the assumption that the PAA-chemisorbed crystal conversion layer is composed of the hybrid phases of zinc phosphate, iron phosphate, and mixed iron and zinc phosphate compounds, both the relative quantities and the identification of these conversion products were studied with X-ray powder diffraction (XRD). The resultant XRD pattern in the diffraction range of 0.883 to 0.167 nm for the powdered samples of a layer removed by scraping the surface is given in Fig. 7. These spacings suggest that the major conversion product is zinc phosphate dihydrate, $Zn_3(PO_4)_2 \cdot 2H_2O$ [14]. The presence of hopeite, $Zn_3(PO_4)_2 \cdot 4H_2O$, phosphophyllite, and iron phosphate, which is reported by Ghali and Potvin [3], could not be clearly identified in the layers derived from the zinc orthophosphate dihydrate-based phosphating solution. However, using AES, the presence of very small amounts of iron phosphate and phosphophyllite were found in the crystalline precoat layers.

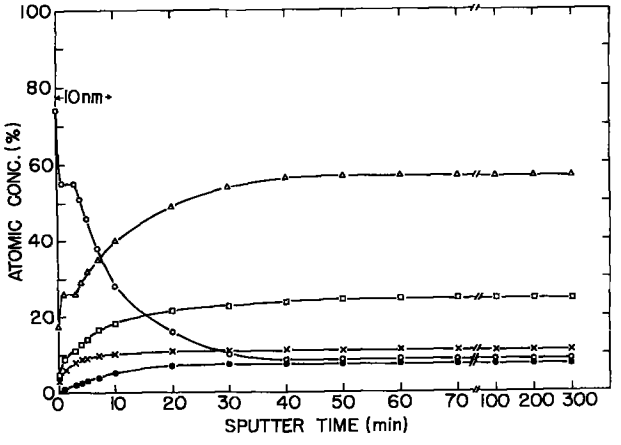

Figure 6 AES atomic concentration depth profile of a complexed conversion layer. △, oxygen; □, zinc; x, phosphorus; ○, carbon; ●, iron.

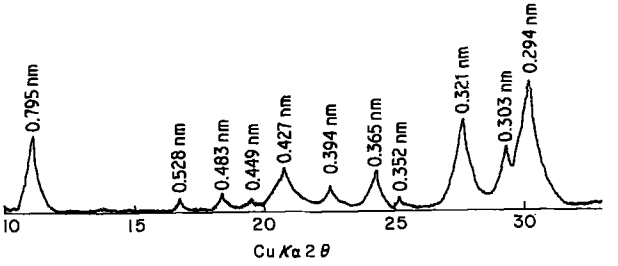

Figure 7 Powder X-ray diffraction pattern of PAA-treated zinc phosphate crystal layer after baking for 24 h at 150° C.

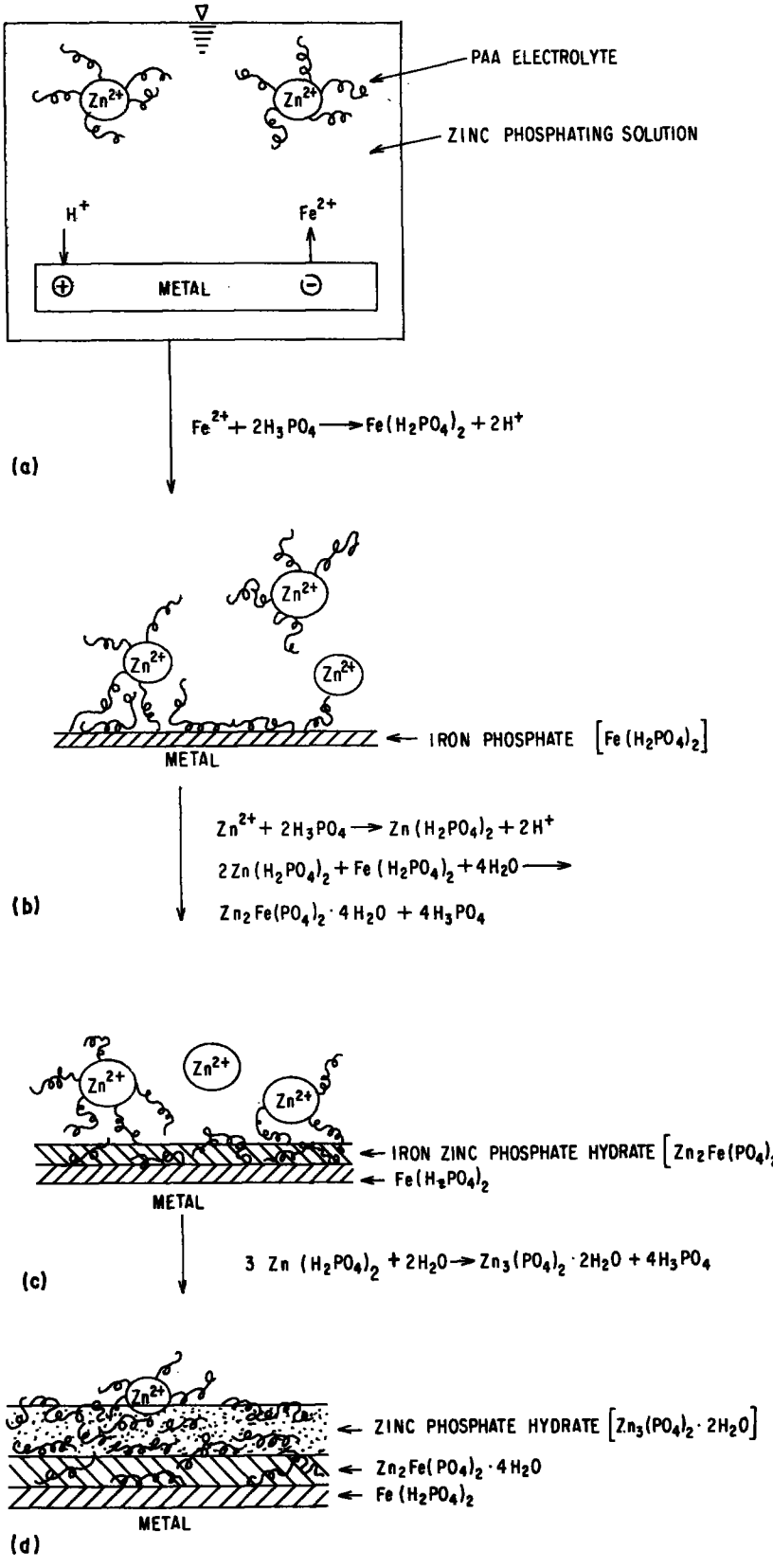

Figure 8 Schematic conversion mechanism of polyelectrolyte–zinc phosphate systems deposited on steel surfaces.

On the basis of these results obtained using various analytical techniques, possible conversion mechanisms for polyelectrolyte-chemisorbed zinc phosphate crystal layers are presented schematically in Fig. 8. As depicted in the figure, the proposed mechanism consists of four steps. In step (a), when the PAA electrolyte is introduced into the zinc phosphating liquid system, the divalent zinc cations are readily complexed with the proton-donating-type carboxylic acid groups in the PAA molecules. The extent of the complex is dependent upon the charge density of the polymer and the concentration of the counterion [15]. It must, therefore, be assumed in the present work that the PAA species are partly dissociated PAA molecules to which a number of zinc ions are bound. This amount of ion binding should permit extensive random coiling of polyanions. Upon immersion of the metal substrate in the acid medium, the substrate surfaces undergo an electrochemical dissolution reaction. The ferrous ions that migrated electrochemically from the substrate surface at the steel-solution interfaces have a strong chemical attraction with the

orthophosphoric acid. This reaction is followed by the precipitation of a thin layer of the first conversion product in terms of iron phosphate, $Fe(H_2PO_4)_2$ [3]. The surface of the precipitated iron phosphate is charged positively because of the large quantity amount of Fe^{2+} ions adjacent to the iron phosphate cores. The surface cationic strength might be strong enough to chemisorb the polyelectrolyte in preference to that of Zn^{2+} ions [see stage (b)]. It is, therefore, postulated that the most logical surface sites to electrostatically attack the ionized COOH groups would be iron ions on the precipitated iron compound surfaces. As a result of chemisorption of ionized PAA segments, some zinc cations masked with PAA macromolecules are released from the PAA–Zn complex formations, and then the dissociated Zn^{2+} ions react with the $2H_3PO_4$ to form zinc phosphate, $Zn(H_3PO_4)_2$. Crystalline zinc iron phosphate hydrate, in terms of phosphophyllite, $Zn_2Fe(PO_4)_2 \cdot 4H_2O$, is probably derived from a reaction between the $Zn(H_3PO_4)_2$ and $Fe(H_3PO_4)_2$ in the aqueous media [16]. Even though the newly precipitated phosphophyllite is superimposed on the PAA-chemisorbed iron phosphate, the segmental chemisorption to the precipitated crystal surfaces by PAA will occur consecutively, as illustrated in step (c). As is evident from the AES and XRD studies, the amount of these iron-rich phosphates, which are precipitated at the begining of the treatment, is much smaller than the zinc phosphate dihydrate, $Zn_3(PO_4)_2 \cdot 2H_2O$, which is the major conversion product of the precoat layers. During the final period depicted in step (d), the residual zinc phosphate is converted into zinc phosphate dihydrate.

From the viewpoint of the polyelectrolyte chemisorption process, the strongly ionized segments of PAA are electrostatically diffused to the positive surface sites of zinc phosphate dihydrate embryos at the beginning of the precipitation. There is no doubt that the high efficiency of segmental chemisorption of organic macromolecules either on newly precipitated nuclei or on growth sites occurring during the primary crystallization processes acts significantly to inhibit the rate of crystal growth. The extent of chemisorption is increased with increasing molecular weight of the PAA. This is related directly to the decrease in size of the crystal or embryonic crystal. The precipitated crystal morphology and habit are also markedly transformed by a strong chemisorption of PAA with an appropriate molecular weight. However, as reported previously [1] when a molecular weight $> 250\,000$ was used, the formed crystals were much smaller than those produced using a lower-molecular-weight PAA. The incorporation of extremely high-molecular-weight PAA completely suppressed the crystal growth by strongly chemisorbing the PAA on the embryonic crystal faces. An alternative explanation for the effect of molecular weight on the crystallization rate is that the high magnitude of entanglement in the PAA–Zn complex systems results in suppression of the electrostatic diffusion of segments to the cationic crystal nuclei surfaces. In other words, it is very difficult for the Zn^{2+} ions existing in a tightly coiled configuration of PAA chains to migrate as free cations from the complex formations. This phenomenon can be expressed in terms of shielding effects which should occur at the strong ionic attractions of PAA with Zn^{2+}. Thus, it is rationalized that the presence of PAA having a particular molecular weight which is representative of less chain entanglement, contributes to the great accessibility by segmental diffusion to the crystal surface sites.

3.2. Durability of adhesive bonds

In order to assess how the surface nature and structure of PAA-chemisorbed zinc phosphate crystal layers affect the durability of adhesive bonds at crystalline precoat-to-polyurethane (PU) topcoat interfacial joints, silica-filled PU polymer was overlaid onto the crystal-precoated steel substrates, and then the PU-coated specimens were subjected to a 0.1 M H_2SO_4 solution at 80° C for up to 10 days. The PU films exhibit excellent chemical resistance to the hot acidic solution, but the conventional zinc phosphate layers are rapidly attacked. All of the edges on the PU-coated plate specimens used in the tests to estimate the bond durability of the PU-to-zinc phosphate adhesive joints were unprotected.

To evaluate adhesion durability at the interface, 180° peel strength tests were conducted at room temperature. For comparison with the adherent forces at PAA–zinc phosphate complex surfaces, two other substrate surfaces, unmodified zinc phosphate and polished plain steel, were also tested. The results from these tests, which were made after various immersion times in the 0.1 M H_2SO_4 solution at 80° C, are presented in Fig. 9. For unexposed specimens, the data indicate that the peel strength of 1.95 kg cm^{-1} developed at the PU–PAA–zinc phosphate joint was considerably higher than at the other joint systems. This can be interpreted as follows: since the functional organic groups such as ionic carboxylate and carboxylic acid are present at the outermost surface sites of the complex crystal layers, the quality of the joints can be attributed to the interfacial chemical bonding between the PU and the functional groups. The presence of such functional groups was found to promote tremendously the adhesive bond at the polymer topcoat-to-crystal precoat interfaces. In contrast, the intrinsic adhesion observed at PU-to-single zinc phosphate joints is attributed to a mechanical interlocking bond produced by anchoring of the polymer as a result of PU liquid resin penetration into the open spaces, and surroundings of the rectangular-type zinc phosphate crystals. The strength value of 0.76 kg cm^{-1} which was developed as result of the mechanical bonding, was $\sim 61\%$ less than that at the PU–PAA–zinc phosphate interfaces. It is also apparent that the physical interlocking formation results in a much stronger bond than that produced with a smooth substrate surface. As indicated in Fig. 9, the lowest strength (0.38 kg cm^{-1}) obtained was when the PU specimens were overlaid on the polished steel surfaces. These results suggest that chemical interactions in polymer-to-polymer adhesion play essential roles in providing strong adhesive forces and chemical stability at the interphase regions.

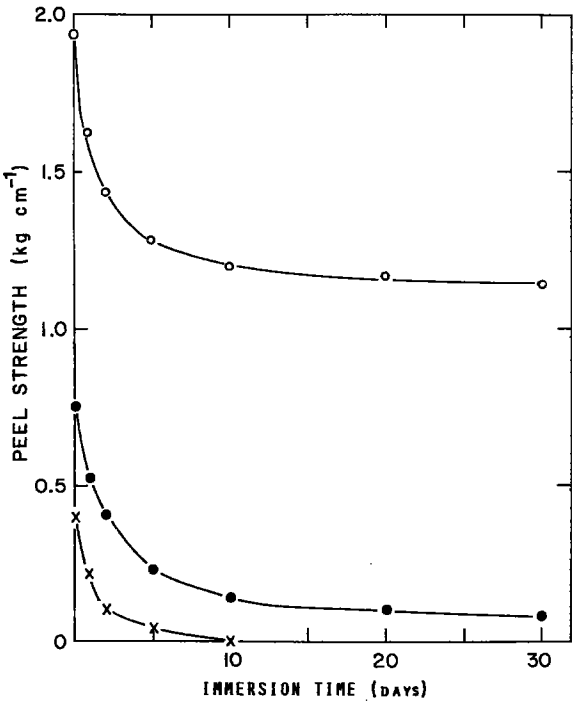

Figure 9 Changes in 180°-peel strength at ○, PU-to-complex zinc phosphate; ●, zinc phosphate; and x, untreated surface joints as a function of immersion time in hot acid solutions.

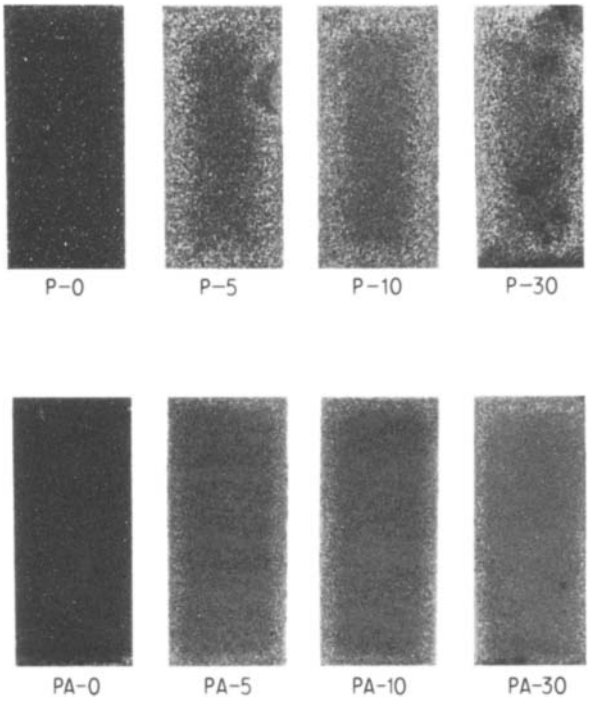

Figure 10 Comparison of (P-) unmodified and (PA-) PAA-modified precoat surface sides after peeling the topcoat from specimens after exposure to 0.1 M H_2SO_4 at 80° C.

After exposure to the hot acidic environment, all specimens exhibited strength reductions as the immersion time was extended. As depicted on the strength–immersion time plot in Fig. 9, noticeable strength reductions were observed within five days. After that, the rate of strength reduction tended to decrease with further exposure. For the PU-to-complex zinc phosphate joint series, the strength was reduced to ~60% of its original value when the specimens were exposed for 30 days. The magnitude and rate of strength regression were considerably greater for the specimens in the PU–zinc phosphate joint system. A reduction to ~30% of the original strength was noted after a five-day exposure. In contrast with these specimens, disbondment failures of PU films bound to polished smooth surfaces occurred very rapidly. After exposure for only 10 days, a clear separation of the PU overlayer from the substrate surfaces was discernible. This implies that the deterioration of polymer–metal bonds is due mainly to poor adhesion. The loss in adhesion under the hydrothermal conditions can most commonly be attributed to the mechanism of blister formation brought about by the penetration of water through the coating to the interface regions.

Fig. 10 shows comparisons between unmodified and PAA-modified zinc phosphate surface sites after PU topcoats were peeled from the interfaces of samples that had been exposed to hot acid solutions for up to 30 days. In Fig. 10, the unmodified and modified zinc phosphate surfaces are designated as samples P and PA, respectively, and the exposure periods in days are signified by the numbers which follow the identification letters. For instance, P-30 corresponds to an unmodified specimen after exposure for 30 days. As is evident from the photographs, the extent of the failure of the interfacial adhesion structure can be visually confirmed from the changes in colour of the crystals on the edges of the precoat sites. For the unmodified zinc phosphate surfaces, the dark areas that represent adhesively bonded interfaces are reduced markedly by extended exposure times. It appears that the chemical degradation of the zinc phosphate crystal itself, brought about by penetration of the acid solution to the interfacial regions, was progressively promoted as the exposure period increased. On the other hand, the degradation failure for the PAA-chemisorbed zinc phosphate precoat surfaces after peeling the PU films was considerably less. Although the 30-day exposed specimen exhibits some colour change at the edges of the substrate surfaces, the interfacial bonding areas were conspicuously larger than those of the unmodified zinc phosphate surface sites at the same exposure ages. These results apparently demonstrate that complex conversion layers derived from a mix solution of zinc phosphate and polyelectrolyte have a high potential for improving the bond durability of polymer-to-metal adhesive joints.

In the crystalline precoat-to-polymer topcoat adhesion studies, the identification of the failure mode can lead to a better understanding of the mechanisms contributing to strong bonds. To obtain information regarding the adhesion failure mode and locus at the topcoat–precoat boundary for the specimens before and after exposure to hot acid solutions, the failure surfaces generated by peeling were explored using low-resolution scanning electron microscopy (SEM) and energy-dispersive X-ray spectrometry (EDX). EDX coupled with SEM has a high potential for the quantitative analysis of any selected elements which exist at solid composite material subsurfaces. This feature can greatly enhance the results, as well as facilitate the interpretation of SEM studies. Both the adhesive PU polymer surface site and the inside crystal precoat surfaces of the peeled specimens,

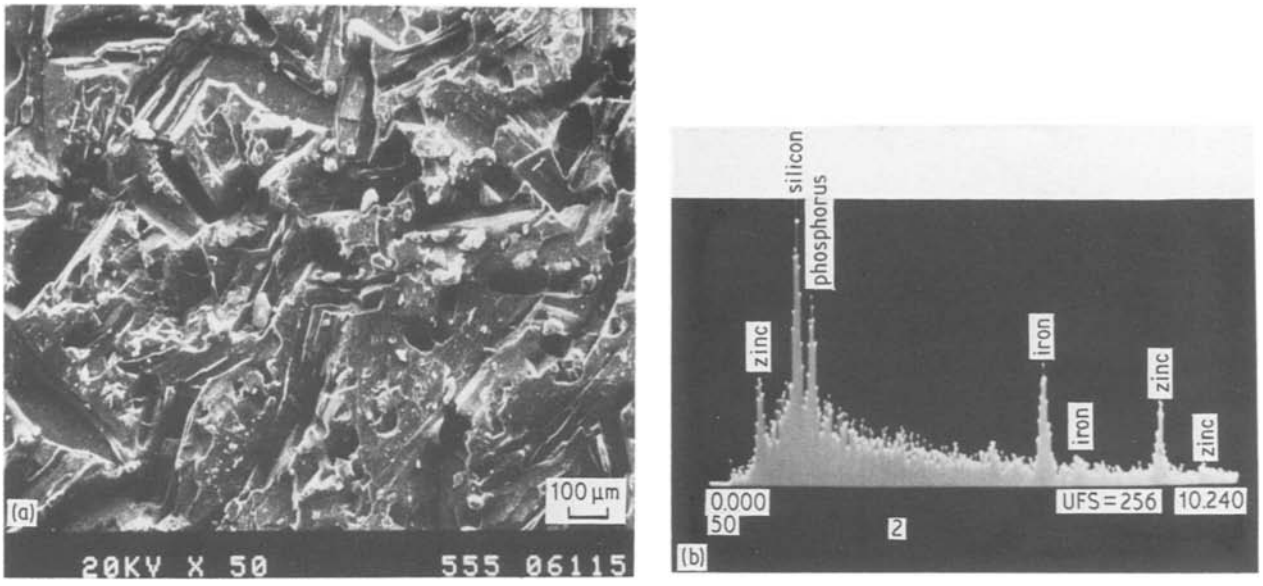

Figure 11 (a) SEM micrograph and (b) EDX of surface side of PU topcoat bonded to zinc phosphate surface before exposure to hot acidic solution. Intensity counts per 50 sec: phosphorus, 218; zinc, 243. Intensity ratio phosphorus: zinc, 0.90.

before and after exposure for 30 days, were subjected to an inspection of the defective mode.

Fig. 11 shows SEM microprobe and EDX elemental analysis of a PU surface removed from an unmodified zinc phosphate surface that was not exposed to the acid solution. The SEM image shows a concave structure with pits and cavities on the interfacial surfaces. The presence of a large number of pits, with rectangular–type shapes can be rationalized in terms of the adhesive failure mechanisms. The adhesion loss in the bonding system might occur near the precoat-to-topcoat interfaces. This failure is representative of the weak adhesive bonding at the PU–zinc phosphate interfacial joints. EDX data to substantiate the failure locus indicate that the predominant element, which is represented by the highest peak intensity, is silicon. Other elements present, but with low peak intensities, are phosphorus, zinc, and iron. The silicon atom is associated with the silica flour used as a filler in the PU polymer. The notable phosphorus, zinc and iron elements probably come from the zinc and iron-based phosphate crystal compounds. The presence of these elements on the peeled PU surfaces indicates a cohesive failure occurring in the precoat subsurface.

From quantitative analyses of the selected elements, the magnitude of cohesive failure in the precoat layers can be estimated. These data consist of the intensity counts per 50 sec of phosphorus and zinc atoms and the elemental ratio of phosphorus-to-zinc peak counts. As seen in Fig. 11, the resultant intensity counts were computed to be 218 and 243 for phosphorus zinc atoms, respectively, and the intensity ratio of P–Zn was 0.90. These values were much lower than those for the adherent surface sites of the precoat (see Fig. 12). Referring to Fig. 12, SEM photomicrographs of the interfacial precoat surface indicate a topography composed of an interlocking structure of rectangular–type crystals, closely resembling that of the

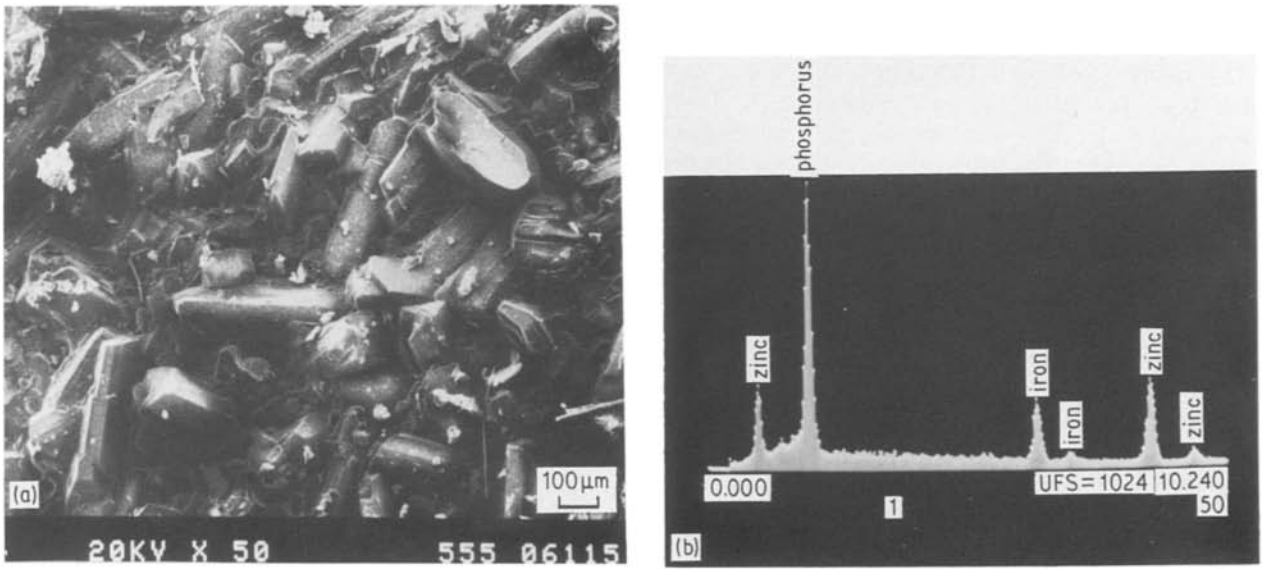

Figure 12 (a) Surface topography with (b) EDX analysis of unexposed zinc phosphate precoat after peeling PU topcoat. Intensity counts per 50 sec: phosphorus, 2688; zinc, 845. Intensity ratio phosphorus: zinc, 3.18.

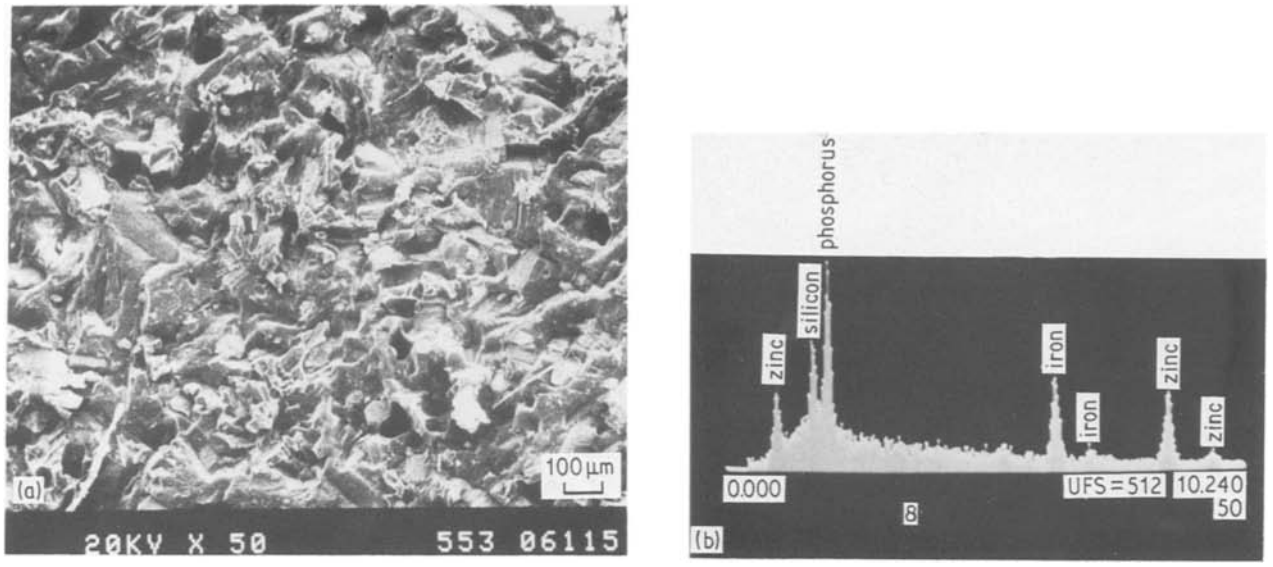

Figure 13 (a) SEM image and (b) EDX analysis of adhesive side of unexposed PU film removed from a PAA-complexed zinc phosphate surface. Intensity counts per 50 sec: phosphorus, 803; zinc, 371. Intensity ratio phosphorus: zinc, 2.16.

conventional conversion crystals. In addition, the absence of the silicon atom in the EDX spectrum indicates that PU was not present on the zinc phosphate precoat surfaces. From the above results, the failure occurring at PU–zinc phosphate joints is probably due to a mixed mode of cohesive (in the precoat) and adhesive failures. In contrast, at the PU-to-PAA-complexed zinc phosphate joints, the topographical features for both the interfacial PU adhesive sites and the complex adhered surfaces for the peeled unexposed specimen were microscopically observed to be quite different. These are shown in Figs 13 and 14. The large-sized pits with rectangular-type shapes that were detected on the PU surfaces bonded to the zinc phosphate could not be seen on the topcoat sites removed from the PAA-modified zinc phosphate precoat surfaces. The EDX peaks indicated that the major chemical constituents of the polymer surface were more likely to be associated with the presence of phosphorus, iron and zinc rather than silicon. In addition, the intensity counts for both phosphorus and zinc atoms and the P : Zn intensity ratio were found to be considerably higher than those obtained from the interfacial topcoat in the PU–zinc phosphate joint systems. It is of particular interest that the ratio value of 2.16 was in the same range as that computed for the complex precoat surface after peeling off the polymer topcoat (see Fig. 14). These experimental data, in conjunction with the SEM image of the rough surface texture for the peeled precoat interfaces, indicate that the locus of the adhesion loss was clearly cohesive since a considerable overlayer of the crystal precoat remained on the PU adhesive surfaces. Hence, the presence of the functional organic species which occupy the most active sites on the precoat, appears to play a major role in promoting good chemical bond performance for polymer topcoat systems. When a direct chemical reaction between the PU polymer and the complex precoat is possible, the interdiffusion aspects at the interfacial regions would be an

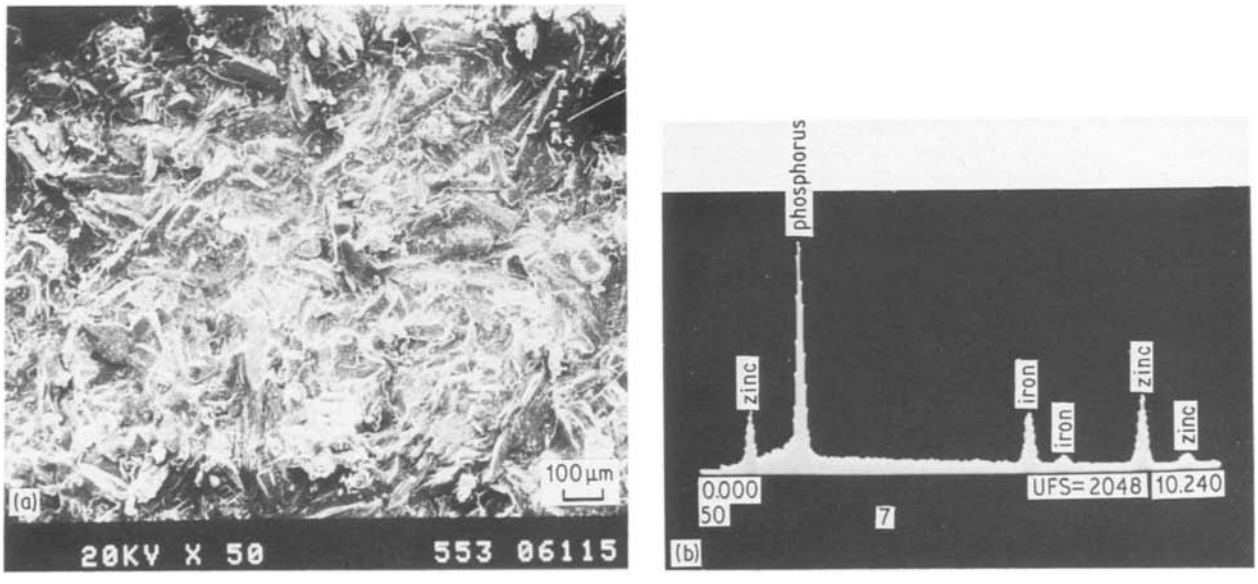

Figure 14 (a) SEM image and (b) EDX analysis of unexposed PAA–zinc phosphate complex layer after peeling PU polymer. Intensity counts per 50 sec: phosphorus, 4070; zinc, 1492. Intensity ratio phosphorus: zinc, 2.73.

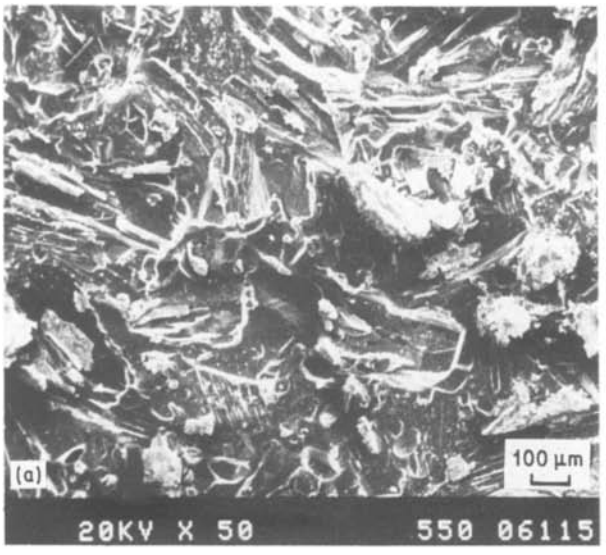

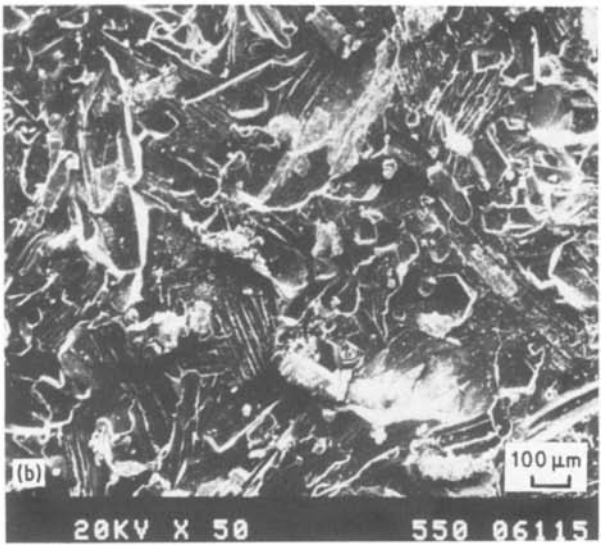

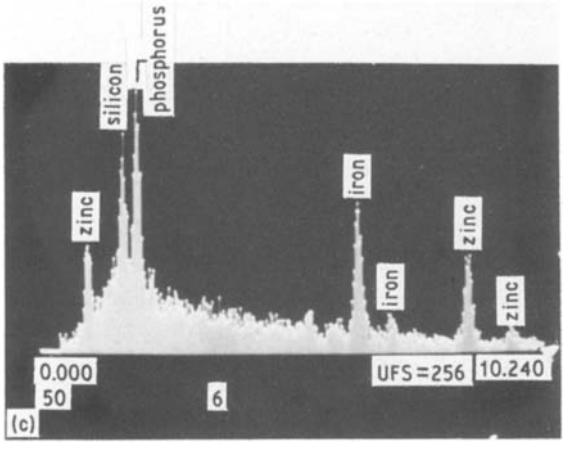

Figure 15 (a) Edge and (b) centre portions of PU films sites removed from zinc phosphate precoat surfaces after exposure for 30 days in acidic solution at 80° C. Intensity counts per 50 sec: (a) phosphorus, 549; zinc, 263; (b) phosphorus, 394; zinc, 230. Intensity ratio phosphorus: zinc, (a) 2.09; (b) 1.71.

important mechanism by which the attractive complex surface promotes adhesive strength. The observed defective mode, which breaks down the crystal precoat system, suggests that the intrinsic strength of the crystal itself is less than that of the adhesion force at the topcoat–precoat joints. The formation of stronger conversion crystals, therefore, is requisite for producing further improvements in the interfacial adhesion bonds.

Similar analyses were performed on samples exposed for 30 days to the acidic environment at 80° C. For PU–zinc phosphate joint specimens, SEM micrographs and EDX analyses at the edge and centre portions of both the adhesive PU and the adherent zinc phosphate interfacial surfaces are given in Figs 15 and 16, respectively. As shown in Fig. 15, the microstructure features disclosed at the edge areas (see Fig. 15a) of the PU surface sites are appreciably different from those at the centre (Fig. 15b). The main difference is the reduced number of rectangular-shaped pits at the edges compared with the number in the centre area. The micromorphological image of the centre area resembles the surface microstructure of the adhesive sites for the unexposed specimens discussed previously. Although the data are not shown in the Figure, the EDX spectrum for the edge areas revealed that the dominant element was phosphorus instead of silicon. It is inferred from these data that some crystal precoat remains on the PU interface after peeling. The relative quantities of the joined crystals were estimated by comparing the elemental quantity values obtained at different locations on the interfacial polymer surface sites. The resultant phosphorus and zinc intensity counts for the edge samples were significantly higher than those for the centre portions. This means that the quantity of zinc phosphate crystal which is transferred to the polymer adhesive sites at the edge regions of the precoat interface is relatively larger than that at the centre areas. The reason for large crystal pieces being left on the polymer interfaces may be as follows: when the PU-to–zinc phosphate adhesion joints come in contact with the hot acid solution, the corrosive fluid readily penetrates through the weak bonding regions at the interfaces. The acid readily attacks the zinc phosphate layers, whereas the PU topcoat at the interface is more durable. The significant progression of the reaction leads to chemical dissolution of the zinc phosphate and the locus of the mechanical disbondment occurs within the highly dissolved precoat layers of zinc phosphate adjacent to the topcoat. Thus, this failing phenomenon results in the presence of the residual crystal on the interfacial PU film surfaces. Since the concept of dissolution failure within the precoating is related directly to the magnitude in susceptibility of the crystal formation to the chemically aggressive fluids, the unmodified zinc phosphate appears to be soluble in the hot acidic solution. Thus, dissolution-induced precoat failure beneath the topcoat seems to be the major factor in the chemical delamination process.

To clarify the dissolution failure mode further, the coated sides of the zinc phosphate precoat were studied in the same manner as described above, and the results are presented in Fig. 16. When compared to the random distribution of angular microcrystals at the centre of the precoat surfaces, the SEM micrograph at the edge of the precoat was characterized by

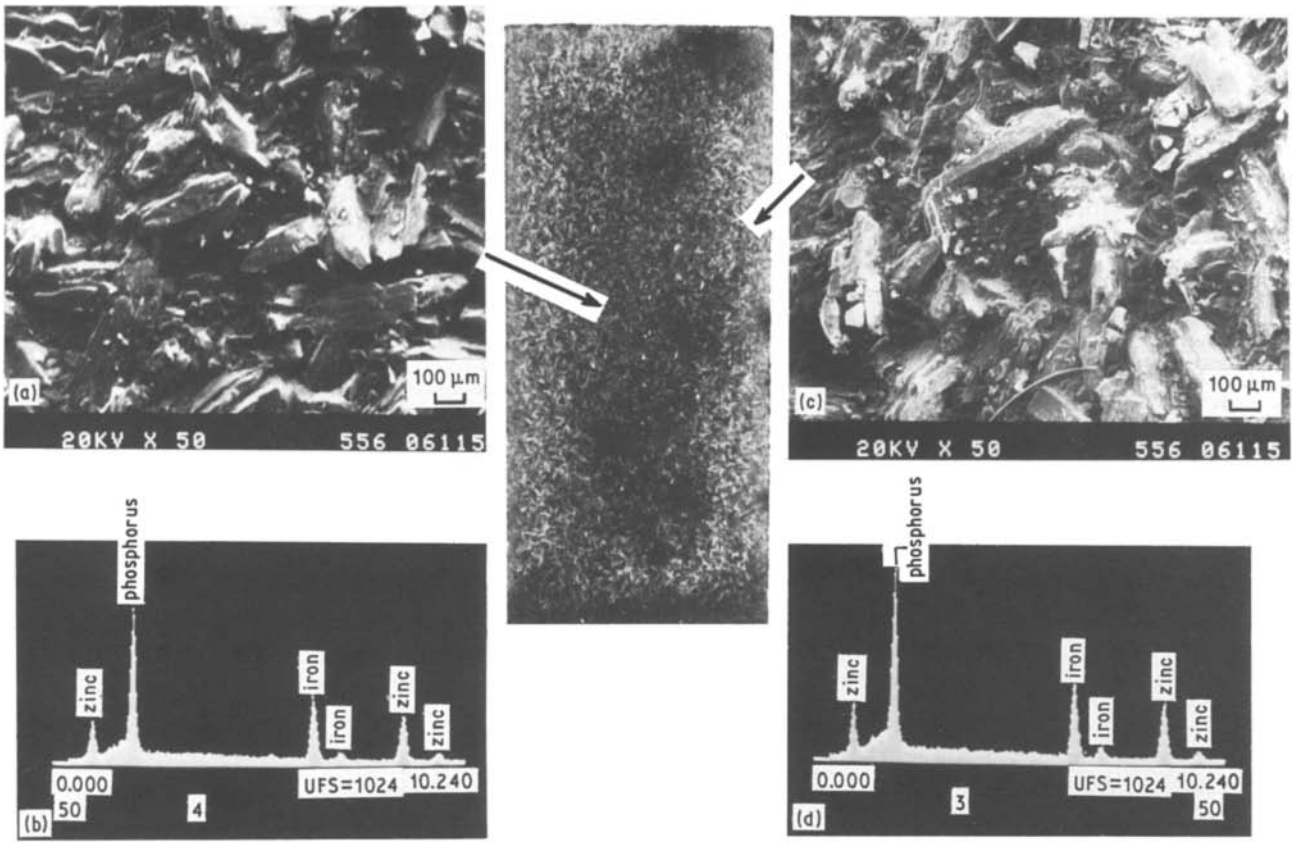

Figure 16 SEM microprobe and EDX at (a, b) centre and (c, d) edge portions of zinc phosphate surface after peeling PU film from specimens exposed for 30 days to hot acidic acid solution. Intensity counts per 50 sec: (a, b) phosphorus, 1711; zinc, 632; (c, d) phosphorus, 1840; zinc, 863. Intensity ratio phosphorus: zinc, (a, b) 2.71; (c, d) 2.13.

a distribution of roundish crystals. The transformation to a roundish shape from the original rectangular-shaped conversion crystals may be due to surface dissolution of the crystals by the acid. The variation in the intensity ratio of P : Zn atoms is associated with the degree of the elemental balance in the zinc phosphate crystal molecules. The most suitable element balance in the original crystal is the P : Zn ratio of 3.18 that was measured for the unexposed precoat interfaces (see Fig. 12). In comparison with this optimum value, the intensity ratio at the edges of the exposed precoat interfaces was reduced by ~33%. In contrast, the reduction in the ratio at the centre area was only 15%, which suggests less dissolution damage to the crystal. The decrease in ratio indicates that the quantity of phosphorus dissolved from the crystal molecules is larger than that of zinc. Consequently, the adhesive loss at the PU–to–zinc phosphate joints for the exposed specimens was due mainly to the more facile dissolution of the zinc phosphate layer adjacent to the interface by the hot acid. However, the chemical dissolution of the zinc phosphate appears to play no significant role in the disbonding mode because the precoat dissolution is seen to occur before disbondment from the PU interface.

Fig. 17 illustrates SEM images and EDX analyses made at the edge and centre portions of PU interfaces that were peeled at the PU-to-PAA-complexed zinc phosphate joints after exposure to the hot acid solution for 30 days. The topographical features of the surfaces at both the edges (see Fig. 17a) and the centre (Fig. 17b) strongly resembled that of the PU removed from the unexposed specimens. However, the intensity counts for both phosphorus and zinc computed at the edges were somewhat lower than those at the centre. The count values for the centre portions are almost equivalent to those of the peeled PU interface for the unexposed specimens (see Fig. 13). Hence, it appears that even though a high degree of interfacial bond forces was developed at the PU–PAA–zinc phosphate interfaces, the precoat layers near the edges might be slightly more susceptible to acid attack, thereby resulting in an appreciable adhesion loss at the joints. The microscopical and elemental data for coated sites of the PAA-adsorbed zinc phosphate are given in Fig. 18. As seen in the micrographs, no conspicuous differences between the surface features at the edge and the centre are apparent. The P : Zn intensity ratios at the edge and the centre were 2.80 and 2.99, respectively, corresponding increases of ~3% and 10% over those obtained from the unexposed PAA–zinc phosphate complex interfaces (see Fig. 14). The enhanced ratio values for the modified zinc phosphate interfaces are in marked contrast to a significantly decreased ratio caused by the dissolution of the unmodified precoat layers. This definitively suggests that the interfaces of complex zinc phosphate bonded strongly with the PU act to significantly restrain the penetration of aggressive acid fluids. Although the PAA structure consisting of a stabilized hydrophobic main chain $(\text{-}CH_2\text{-}CH\text{-})n$ and hydrophilic pendent (COOH) groups was transformed into complex formations by the divalent metallic ions, the complexes formed at the outermost surface sites of the precoat layers were

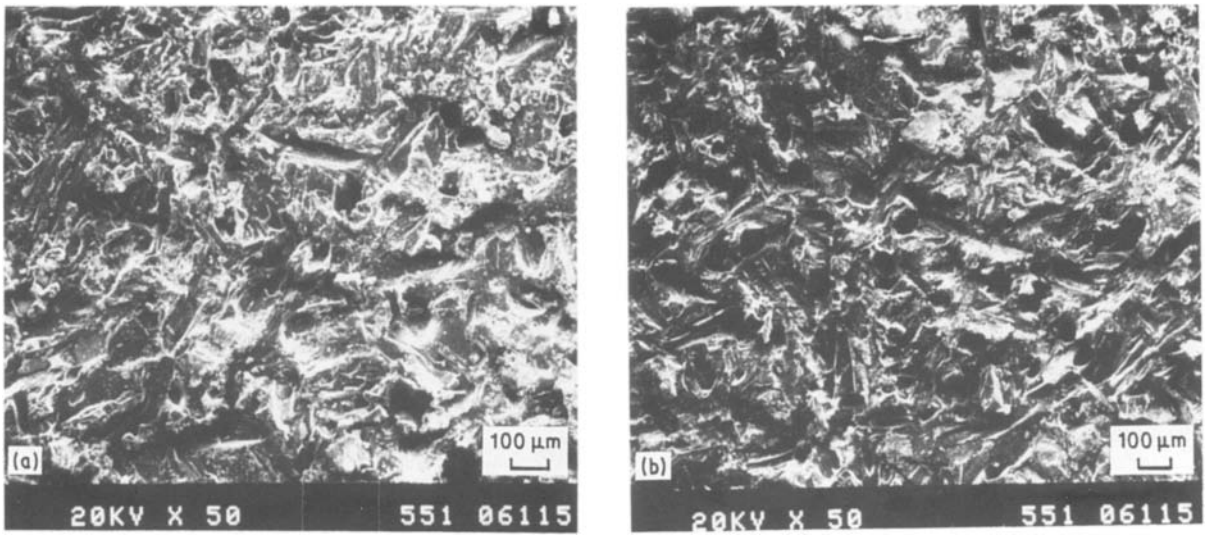

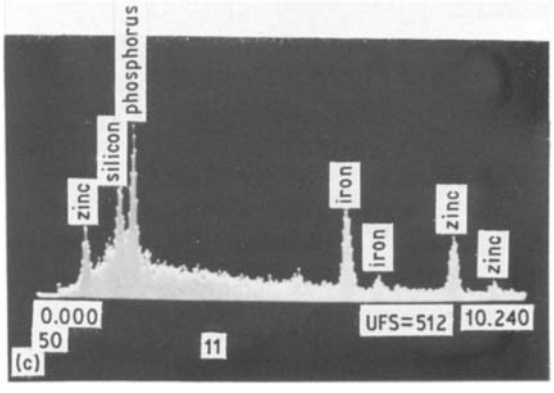

Figure 17 (a) Edge and (b) centre parts of PU surface sites bonded to PAA-zinc phosphate complexes after 30-day exposure. Intensity counts per 50 sec: (a) phosphorus, 644; zinc, 308; (b) phosphorus, 745; zinc, 313. Intensity ratio phosphorus: zinc, (a) 2.09; (b) 2.38.

identified to have an unstable hydrophilic nature. However, the chemical interaction at the PU-to-complex interfacial boundary might form new reaction products which possess hydrophobic characteristics less susceptible to the acidic fluids. This hydrophobic structure formed at the interface appears to play an important role in achieving a long-term bond durability in chemically aggressive environments. From the above results, it appears that the PAA's effectiveness in improving the bond durability of zinc phosphate adhesive joints is due to its ability to convert into a hydrophobic material by chemical bonding with the polymeric topcoat and its coupling function which promotes an adhesive force at the topcoat–precoat interfaces.

4. Conclusions

In deposition processes for PAA–zinc phosphate complex conversion precoats on cold-rolled steel surfaces, the positive surface sites of multiple phosphate crystal embryos at the beginning of the precipitation were strongly chemisorbed by the anionically charged segments of PAA electrolytes. The electrostatically segmental chemisorption of polyanions either on newly precipitated nuclei or on growth sites during the primary crystallization processes acts to suppress and delay the crystal growth. From this current work and the previous results, it appears that the introduction of polyelectrolytes with a high molecular weight $> 250\,000$ completely inhibits the crystal growth because of the stronger chemisorption of PAA on the embryonic crystal faces. When PAA with a molecular weight of 104 000 was electrostatically or chemically diffused into the precipitated crystal layers, the depth-composition profile of the resulting deposition layers indicated the presence of the following three discernible phases:

1. highly concentrated polyelectrolyte regions within the first ~ 5 nm thickness;
2. poorly crystallized zinc and iron phosphate compounds caused by chemisorbing an abundant PAA in the depth range of ~ 5 to ~ 35 nm;
3. the presence at a depth below ~ 35 nm of a well-crystallized phase containing a constant quantity of internally diffused PAA.

The major conversion product in the well-crystallized phases was identified to be the zinc phosphate dihydrate. The iron phosphate and phosphophyllite are present as a minor phase in crystalline phase assemblages.

The chemical state at the outermost surface sites of the PAA-chemisorbed zinc phosphate precoat layers was composed of the ZnO, P_2O_5, HPO_3, and functional organic groups. The presence of functional organic species such as ionic carboxylate and carboxylic acid groups contributed to the dramatic improvement in the adhesive force at the crystalline precoat-to-polymeric topcoat interfacial joints. The major role in promoting a good interfacial bond performance of the surface chemical nature of the precoat systems was due to the following two factors. One was to act as a primer which can be compatible with the adhesive, and the other serves as a chemical coupling function connecting between the organic adhesive and the inorganic zinc phosphate. The former in terms of an internal lubricant or wetting agent would enhance the flowability of the liquid resin which results in improved bond properties at the interfaces.

The inherent stability of the chemical bonding at the polymer-to-complex zinc phosphate interfaces was found to play the key role in enhancing the bond

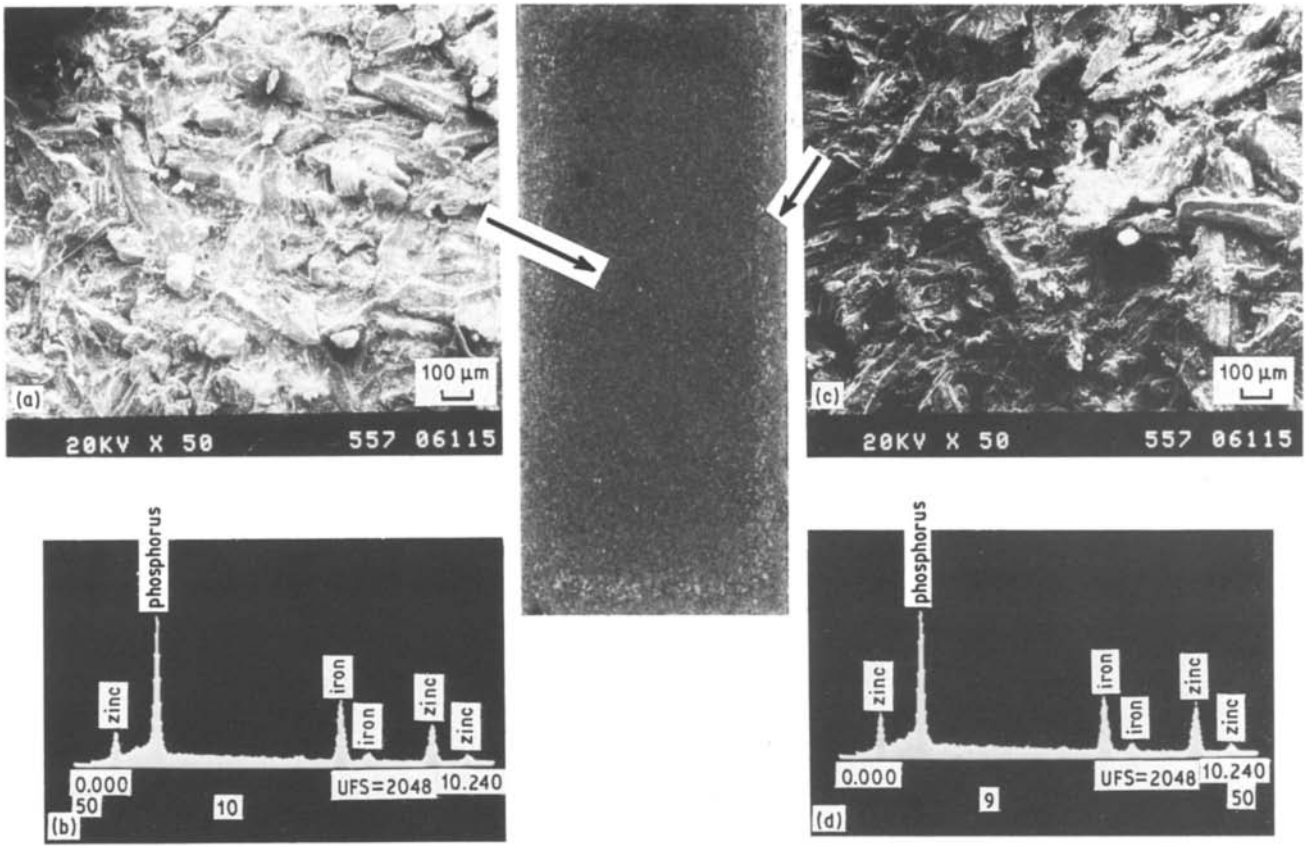

Figure 18 Surface morphological and elemental figures, of PAA–zinc phosphate complex precoat after peeling PU polymer for 30-day exposed specimens; (a, b) centre and (c, d) edge portions. Intensity counts per 50 sec: (a, b) phosphorus, 3171; zinc, 1061; (c, d) phosphorus, 3015; zinc, 1078. Intensity ratio phosphorus: zinc, (a, b) 2.99; (c, d) 2.80.

durability of metal adhesive joints. In the exposure tests of PU topcoat-overlaid PAA-modified and PAA-unmodified zinc phosphate specimens in hot H_2SO_4 solutions at 80° C for up to 30 days, the resultant peel strength reduction for 30-day immersed PU–PAA–zinc phosphate joint systems was noted to be only ~41%, as compared to ~70% for PU–zinc phosphate systems. The adhesion failure mode and locus at the interfacial boundary for the peeled specimens before and after exposure, were consequently proposed in Fig. 19. As seen in the figure, the failure at the PU–zinc phosphate joint before exposure was through a mixed mode of adhesive and cohesive (in the precoat) failures. In contrast, the locus of adhesive loss of PU–PAA–zinc phosphate joint systems was identified to be clearly cohesive, thereby increasing the interfacial bond strength. For the specimens after 30 day exposure, the adhesive loss for the PU–zinc phosphate systems was due mainly to the dissolution of the zinc phosphate layer adjacent to the interface by the penetration of acid solutions. However, the failure mode for the exposed PU–PAA–zinc phosphate was confirmed to be cohesive, similar to that for the unexposed specimens. This suggests that the

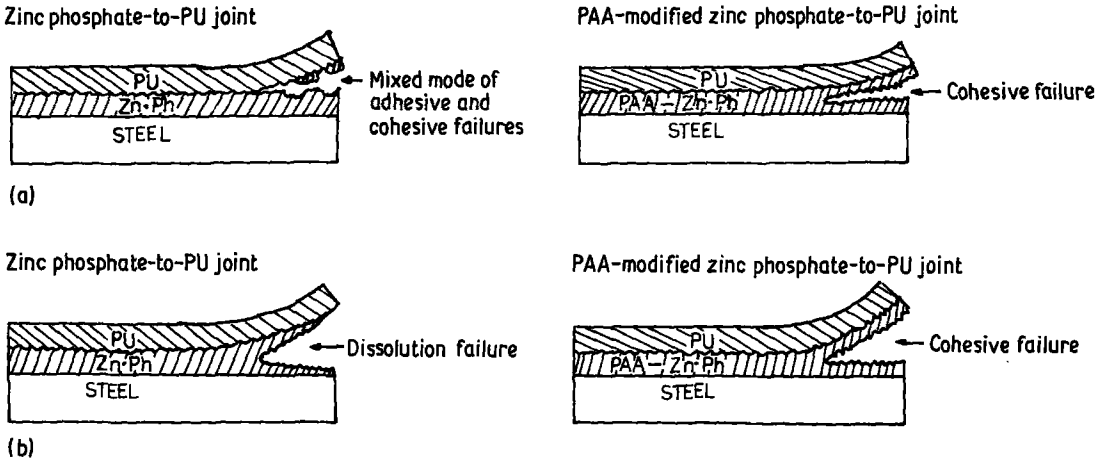

Figure 19 Proposed failure modes for PU–PAA–zinc phosphate and PU-zinc phosphate/joint systems before and after exposure to 0.1 M H_2SO_4 at 80° C for 30 days.

hydrophobic structure formed by the interfacial chemical attraction between the PU and the functional organic species plays an important role in achieving a long-term bond durability at metal adhesive joints that will be subjected to chemically corrosive environments.

Acknowledgements

This work was performed under the auspices of the US Department of Energy, Washington DC, under contract No. DE-AC02-76CH00016, and supported by the US Army Research Office Program MIPR-ARO-112-86.

References

1. T. SUGAMA, L. E. KUKACKA and N. CARCIELLO, *J. Mater. Sci.* **19** (1984) 4045.
2. T. SUGAMA, L. E. KUKACKA, N. CARCIELLO and J. B. WARREN, *J. Appl. Polym. Sci.* **30** (1985) 2137.
3. E. L. GHALI and R. J. A. POTVIN, *Corros. Sci.* **12** (1972) 583.
4. J. B. LAKEMAN, D. R. GABE and M. O. W. RICHARDSON, *Trans. Inst. Metal Finishing* **55** (1977) 47.
5. R. A. IEZZI and H. LEIDHEISER Jr., *Corrosion* **37** (1981) 28.
6. T. SUGAMA, L. E. KUKACKA, N. CARCIELLO and J. B. WARREN, *J. Appl. Polym. Sci.* **30** (1985) 4357.
7. J. E. CRAWFORD and B. R. SMITH, *J. Colloid. Interface Sci.* **21** (1966) 623.
8. C. H. NESTLER, *J. Colloid. Interface Sci.* **26** (1968) 10.
9. T. SUGAMA, L. E. KUKACKA, N. CARCIELLO and J. B. WARREN, *J. Appl. Polym. Sci.* **32** (1986) 3469.
10. H. LEIDHEISER Jr., *Corrosion* **38** (1982) 374.
11. O. D. GONZALEZ, P. H. JOSEPHIC and R. A. ORIANI, *J. Electrochem. Soc.* **121** (1974) 29.
12. C. D. WAGNER, W. M. RIGGS, L. E. DAVIS, J. F. MOULDER and G. E. MUILENBERG, Handbook of X-Ray Photoelectron Spectroscopy (Perkin-Elmer Corporation, 1979) p. 19.
13. *Idem, ibid.* p. 84.
14. Joint Committee on Powder Diffraction Standards, Card 30-1491.
15. M. L. MILLER, The Structure of Polymers (Reinhold, New York, 1966) p. 580.
16. J. A. KARGOL, D. L. JORDAN and A. R. PALERMO, *Corrosion* **39** (1983) 213.

Received 25 March
and accepted 5 June 1986